

Abundant water-soluble calcium coatings on fine Asian dust particles

Tafeng Hu¹, Niu Jin², Yingpan Song¹, Feng Wu¹, Jing Duan¹, Yuqing Zhu¹, Hong Huang², Yu Huang¹, Junji Cao³, Daizhou Zhang⁴

¹State Key Laboratory of Loess Science, National Observation and Research Station of Regional Ecological Environment Change and Comprehensive Management in the Guanzhong Plain, Institute of Earth Environment, Chinese Academy of Sciences, Xi'an 710061, China.

²School of Resources and Environment, Nanchang University, Nanchang, 330031, China.

³Institute of Atmospheric Physics, Chinese Academy of Sciences, Beijing 100029, China.

⁴Faculty of Environmental and Symbiotic Sciences, Prefectural University of Kumamoto, Kumamoto 862-8502, Japan.

10 *Correspondence to:* Junji Cao (jjcao@mail.iap.ac.cn); Daizhou Zhang (dzzhang@pu-kumamoto.ac.jp)

Abstract. The dissolution behavior of atmospheric calcium (Ca) mineral dust released from arid regions and their climate impacts via buffering effects are highly dependent on their size-resolved mineralogical composition. Due to the inherent complexity of mineral dust, tracing the chemical forms and mixing states of Ca minerals at single-particle level remains challenging. In this study, an automated microanalysis technique was employed to characterize the physicochemical properties of 43,990 individual mineral dust particles generated by saltation-sandblasting processes in two deserts, along with their residual 42,306 particles after water dialysis. Both the total dust and the Ca-containing particles exhibited a modal peak in the submicron size range, before and after dialysis. After dialysis, 56.9 % to 88.2 % (by number) of the calcium-containing dust particles lost their soluble calcium components. These water-soluble elemental Ca accounted for 19.6–41.9 % of the mass of elemental Ca in both the Taklimakan and Gobi deserts. In addition, more than 73.2 % of Ca-O-rich and Ca-S-containing particles occurred as water-soluble surface coatings on other minerals and were effectively removed by dialysis. The results provide a realistic constraint for assessing the abundance of water-soluble Ca coatings on fine particles emitted from two Asian deserts.

25 **1 Introduction**

Mineral dust represents a major component of atmospheric aerosol, accounting for up to 75 % of the global aerosol mass (Choobari et al., 2014). Global dust emissions are estimated from $2000 \pm 400 \text{ Tg yr}^{-1}$ (Kok et al., 2021a) to $2566 \pm 1996 \text{ Tg yr}^{-1}$ (Zhao et al., 2023), with Asia contributing from 25–30 % (Kok et al., 2021b) to ~40 % (Kok et al., 2023) of the total. Through direct effects, mineral dust perturbs Earth's radiative balance (Choobari et al., 2014; Adebiyi et al., 2023) primarily via scattering (Nousiainen, 2009), though it also exhibits considerable absorption depending on its mineral composition and mixing state (Falkovich et al., 2001; Formenti et al., 2011). Through indirect mechanisms, mineral dust acts as ice-nucleating particles (INPs) and cloud condensation nuclei (CCN) (Schepanski, 2018), thereby modifying cloud properties, albedo, and precipitation patterns (Engelbrecht and Derbyshire, 2010; Pye, 2015). The deposition of mineral dust onto terrestrial and marine ecosystems supplies essential micronutrients, stimulating primary productivity and affecting both ecological dynamics and marine biogeochemistry (Quigg, 2016; Mahowald et al., 2018). The transport distance, transformation, and environmental impacts of atmospheric mineral dust are strongly governed by its size distribution, chemical composition, and mixing state (Knippertz and Stuut, 2014). Although the fine fraction (diameter $< 2.5 \mu\text{m}$) constitutes only 5–20 % of emitted dust mass (Formenti et al., 2011; Choobari et al., 2014), it disproportionately contributes to the global particle population (Mahowald et al., 2014) and dominates long-range transport due to its prolonged atmospheric lifetime (Uno et al., 2009; Pye, 2015). A major emission mechanism is saltation-driven sandblasting (Shao et al., 1993), in which sand-sized particles (50–500 μm) bombard the surface, releasing fine dust even at wind speeds below the direct entrainment threshold of fine dust particles (Alfaro, 2008; 2022). This process amplifies dust emission fluxes by 3–10 times (Parajuli et al., 2016) and is responsible for over 75 % of global fine dust emissions (Grini and Zender, 2004). Crucially, sandblasting largely modifies the dust's physical and chemical characteristics compared to the parent soil. It enriches the fine mode (Alfaro et al., 1997; Grini et al., 2002) and preferentially liberates soluble salts and clay coatings from soil aggregates, thereby elevating water-soluble ions (e.g., Ca^{2+}) in the aerosol (Wu et al., 2022). The resulting size distribution governs atmospheric transport duration and influences each mineral's global distribution (Panta et al., 2022), while chemical alterations enhance dust hygroscopicity, reactivity, and radiative efficiency, intensifying its role in climate and biogeochemical cycles.

Among the various chemical components of dust, atmospheric calcium (Ca) predominantly originates from soil dust particles and sea salts. Its buffering effects in the atmosphere and carbon dioxide fixation in the ocean can modify acidity across multiple spheres of the earth (Tipper et al., 2016). Common Ca-containing minerals in natural dust such as calcite (CaCO_3) can rapidly neutralize acidic species in precipitation or upon deposition in terrestrial and marine environments (Cao et al., 2005). Calcite, as a ubiquitous Ca-rich mineral in arid soils, constitutes 5–15% of dust from major source regions (Engelbrecht and Derbyshire, 2010; Knippertz and Stuut, 2014). It is a potent alkaline agent that neutralizes acids (e.g., H_2SO_4 , HNO_3) during transport (Wang Y. et al., 2012), moderating aerosol pH and influencing reactivity (Usher et al., 2003; Craig et al., 2018). During these

acid neutralization processes, calcite dissolution is kinetically controlled and not instantaneous, the extent of its chemical aging—and thus its buffering efficiency—is strongly influenced by atmospheric acidity and transport timescale (Morse et al., 2007). However, the buffering capacity of these particles is not uniform and is intrinsically governed by their dissolution behavior, which varies with particle size and heterogeneity. Evidence from multiple research approaches highlights the critical importance of size-resolved mineralogical composition: it has been shown to govern atmospheric acidity in trend analyses (Ren et al., 2011), to modify CCN-activity in laboratory experiments (Sullivan et al., 2009), and to regulate marine alkalinity in surface waters through field observations (Carter et al., 2014; Su et al., 2020). Moreover, the apparent hygroscopicity of calcium-rich dust is controlled by its chemical mixing state, a property determined by source mineralogy and chemical transformations during atmospheric transport (Sullivan et al., 2009). Following deposition, the dissolution behavior of atmospheric calcium carbonate remains sensitive to the physical and mineralogical characteristics of the dust, as observed both regionally along oceanic transects (Feely et al., 2002) and at a global scale (Sulpis et al., 2021). Therefore, the size-resolved mineralogical composition of atmospheric dust serves as a key link between continental dust sources and global climate feedbacks via the calcium cycle, a claim supported by both modern (Maher et al., 2010) and paleoclimate studies (Tipper et al., 2016).

The heterogeneous chemistry of individual dust particles, which is essential to their atmospheric processing and dissolution behavior, varies significantly with source region (Krueger et al., 2004). A particle's ability to uptake sufficient water to activate into a cloud droplet is governed primarily by its size and soluble hygroscopic content (McFiggans et al., 2006). Modern analytical techniques enable direct observation of atmospherically-processed calcium carbonate dust particles, revealing complex single-particle morphologies and reaction pathways (Laskin et al., 2005). Laboratory studies further indicate that the hygroscopic behavior of specific calcium salts reflects complex internal mixtures (Guo et al., 2019), which control the dissolution kinetics and acid-buffering efficiency of dust in the atmosphere and after deposition into aquatic environments (Usher et al., 2003). A mechanistic understanding of these micro-scale processes is critical for accurately modelling the global calcium cycle (Fantle and Tipper, 2014; Gussone et al., 2016) and dust's influence on the carbon cycle (Jickells et al., 2014; Steiner et al., 2021). However, tracing the chemical forms and mixing states of calcium-containing dust at the single-particle level remains challenging, as these properties evolve continuously during atmospheric transport.

Therefore, accurately predicting the climate impacts of realistic calcium-containing mineral dust aerosols requires detailed data on their size-resolved chemical composition and mixing state, as well as a fundamental understanding of compound–water interactions. In this study, laboratory-generated mineral dust particles produced by the saltation-sandblasting mechanism were collected and subjected to water dialysis treatment. Using computer-controlled scanning electron microscopy (CCSEM), the same set of individual dust particles was analyzed before and after water dialysis, enabling estimation of the number emission flux of calcium-containing particles and the mass of water-soluble calcium components. Changes in the particle size distribution, shape factors, and mixing states of all Ca-O-rich and Ca-S-containing dust particles were quantified. The resulting emission flux and mixing state data provide key insights for assessing the potential climate and carbon cycle impacts of these mineral dust aerosols.

90 2 Methodology

2.1 Sample Collection

Sand dunes and gravel soils are recognized as major sources of atmospheric dust in the arid regions of northern China (Laurent et al., 2005; Mikami et al., 2005; Wang X. et al., 2012; Sweeney et al., 2016; Zou et al., 2018). To this end, four representative soil samples were collected from these two surface types in the Taklimakan Desert and the Gobi deserts (Fig. S1). The
95 Taklimakan Desert is located in the Tarim Basin and covers an area of more than 337,000 km², about 85 % of which is shifting sand dunes in the central area of the basin, surrounded by a zone of gravels called the gobi belt (El-Baz, 1984; Sun and Liu, 2006). The Alashan (Alaxa) Plateau is located in the west part of Inner Mongolia, with the Badanjinlin (Badain Jaran) Desert (49,000 km²) in the mid-west of the plateau, the Tenggeli (Tengger) Desert (42,700 km²) in the south, and the Wulanbuhe (Ulan Buh) Desert (10,000 km²) in the south. Those Gobi deserts on the Alashan Plateau are considered as important mineral
100 dust emission source regions in arid and semiarid China (Shao and Dong, 2006; Wang et al., 2008). Detailed information on the locations and surrounding geomorphology of the sampling sites is listed in Table S1. Surface soil (0-5 cm depth) was collected using a 20 cm × 5 cm plastic shovel. Following collection, samples were placed into self-sealing polyethylene bags (Fig. S1), air-dried in the laboratory, and then stored at room temperature without sieving. For each sample, the coordinates, type, and description of the surroundings were documented.

105 2.2 Laboratory Dust Generation

Mineral dust aerosol particles were generated from soil samples by means of a dust resuspension chamber system. The system generates dust particles from the desert surface soils based on the mechanism of dust saltation and sandblasting processes (Wu et al., 2022), which showed a consistent trend in particle size distribution and chemical composition with field dust aerosols (Wu et al., 2023). Dust particles were mobilized by a rotating annular blade in the chamber of the system, with an equivalent
110 friction velocity of 0.54 m s⁻¹ (Etyemezian et al., 2007), and the resuspended particles were led out into a cylindrical sampling cavity. Total suspended particulate (TSP) samples were collected through the sampling port of the cavity onto 47 mm polycarbonate filters (pore size of 0.2 μm, Whatman International Ltd., Maidstone, UK) using a portable aerosol sampler (Model mini-Vol, Airmetrics Corp., Springfield, OR, USA). The operating flow rate of sampling was 5 L min⁻¹. The sampling duration for each sample varied between 1 and 5 minutes to minimize particle overlap on the filters, depending on real-time
115 TSP mass concentrations measured using a DustTrak aerosol monitor (Model 8530, TSI Inc., Shoreview, MN, USA). Procedural blanks were collected concurrently from the resuspension chamber in the absence of samples. After sampling, each filter was placed in a plastic cassette and stored at 5 °C until analysis.

2.3 Microanalysis and water dialysis

A rectangular section with the size of 10 mm × 10 mm was cut from the central area of the filter by a stainless-steel scissor
120 and mounted onto an aluminum stub with conductive adhesive carbon tape for CCSEM analysis and water dialysis process.

Before microanalysis, the samples were coated with carbon for particle conductivity. For each sample, all individual mineral dust particles dispersed in over 100 fields of view ($100\ \mu\text{m} \times 100\ \mu\text{m}$ for each field, aligned in a rectangular array) were physicochemically characterized one by one using a field emission gun scanning electron microscope (MAIA3, Tescan, Brno, Czech Republic) equipped with dual energy dispersive X-ray (EDX) detectors (Xflash 6-60, Bruker, Karlsruhe, Germany).
125 Automated microanalysis was performed by CCSEM analysis software (IntelliSEM, RJ Lee Group, Inc., Monroeville, USA) to obtain particle images, size distribution, morphological parameters (e.g., aspect ratio, roundness, and form factor), and elemental compositions. The quantitative analysis by the CCSEM provided reproducible sizing and identification of individual particles based on large numbers ($> 10,000$ in this study) for statistical counting (Mamane et al., 2001; Castillo et al., 2019). Following microanalysis, the stubs were transferred to a stainless-steel settlement dish (Okenshoji Co. Ltd.). Dialysis with
130 Milli-Q water was then conducted following the method of Zhang and Iwasaka (2004) to remove water-soluble components from the dust particles (Fig. S2) without disturbing their original locations (Fig. S3). The CCSEM system then relocated the same set of over 100 pre-analyzed fields of view and performed automated microanalysis under consistent operating conditions. This ensured that all particles analyzed post-dialysis were identical to those characterized before-dialysis, guaranteeing the comparability of measurements. The physical (size and morphology) and chemical (elemental compositions) properties of the
135 dust particles were compared to confirm their alteration in shape and composition after dialysis. In addition to the automated microanalysis, manually operated EDX mapping was performed on all individual Ca-O-rich and Ca-S-containing particles to compare their mixing states.

Particle diameters were measured using a rotated-feret box technique (ASTM F1877-16), with a box or a caliper being clockwise rotated around the particles and particle length being recorded at each orientation. Average diameter (D_{avg}) is the
140 arithmetic average of all the 90 measurements, and the maximum diameter (D_{max}) and the minimum diameter (D_{min}) are the largest and smallest of all the measurements, respectively. The aspect ratio (AR) of the particle is the ratio of D_{max} to its perpendicular width. The roundness (R) of a particle is a measure of how closely a particle resembles a circle and has a value between 0 and 1, where the R of a perfectly circular particle is 1. Roundness was calculated using the following formula:

$$R = \frac{4A}{\pi D_{\text{avg}}^2}, \quad (1)$$

145 where A is the projected area of the particle. The form factor (FF), which is a dimensionless number sensitive to the irregularities in particle edges, i.e., the variations in roughness of a particle outline, was calculated using

$$FF = \frac{4\pi A}{p^2}, \quad (2)$$

where p is the perimeter of the particle outline.

For the quantitative elemental analysis, the weight percentages of elements from carbon (C) to lead (Pb) were determined
150 based on their characteristic X-ray signals, which were fitted to Gaussian distributions (Okada and Kai, 2004). The relative weight percentage of each element ($Z > 6$, Carbon) in a particle is the ratio of its peak area to the total peak areas of all detected

elements. Individual mineral dust particles were classified into several mineralogical categories according to how the particle's elemental composition followed the empirical formula of a specific mineral (Hu et al., 2022). The particle classification rules are listed in Table S2. The empirical formula and elemental composition information are available in the handbook of mineralogy (Cook, 2001) and several online databases at <https://duffy.princeton.edu/mineralogy-and-crystallography-databases>.

Assuming an ellipsoidal geometry, the volume of each particle was calculated from its measured major (D_{\max}) and minor (D_{\min}) axial diameters. The particle mass (m) was subsequently determined as the product of its volume and its estimated density (ρ), where ρ was inferred from the particle's EDX elemental composition (Ault et al., 2012). In each mineral dust sample, the total particle count (N_{tot}) and total mass (m_{tot}) were defined as the number and mass of all particles prior to dialysis, respectively. The number of water-soluble Ca-containing particles ($N_{\text{sol-Ca}}$) was derived from the difference in Ca-containing particle counts before versus after dialysis. Correspondingly, the mass of water-soluble elemental Ca ($m_{\text{sol-Ca}}$) was calculated as the difference in total elemental Ca mass before and after dialysis. Consequently, their emission fluxes from mineral dust generated via saltation-sandblasting processes is given by:

$$k_F = \frac{1}{(v \times t)} \times \frac{A_{\text{filter}}}{A_{\text{view}}} \times \frac{Q}{A_{\text{chamber}}} \quad (3)$$

$$F_{N(\text{tot})} = N_{\text{tot}} \times k_F \quad (4)$$

$$F_{m(\text{tot})} = m_{\text{tot}} \times k_F \quad (5)$$

$$F_{N(\text{sol-Ca})} = N_{\text{sol-Ca}} \times k_F \quad (6)$$

$$F_{m(\text{sol-Ca})} = m_{\text{sol-Ca}} \times k_F \quad (7)$$

Where, k_F combines chamber sampling and CCSEM observation parameters in the flux estimation, including v is the air flow rate of the aerosol sampler (5 L min^{-1}), t is the sampling duration for the resuspension samples (min), A_{filter} is the total area of the sampling filter (a fixed area of 11.34 cm^2 in this work), A_{view} is the total area analyzed by CCSEM on the sampling filter (mm^2), Q is the exhaust airflow rate from the resuspension chamber (a fixed rate of 250 L min^{-1}), and A_{chamber} is the bottom area of the resuspension chamber (a fixed area of 0.255 m^2). $F_{N(\text{tot})}$ is the number emission flux of total mineral dust particles from these two Asian deserts via saltation-sandblasting processes (unit: $\text{particles m}^{-2} \text{ d}^{-1}$), and $F_{m(\text{tot})}$ is their mass emission flux ($\mu\text{g m}^{-2} \text{ d}^{-1}$). The number emission flux, $F_{N(\text{sol-Ca})}$, and the mass emission flux, $F_{m(\text{sol-Ca})}$, represent the emission of water-soluble Ca-containing particles and water-soluble elemental Ca itself, with units of $\text{particles m}^{-2} \text{ d}^{-1}$ and $\mu\text{g m}^{-2} \text{ d}^{-1}$, respectively.

2.4 Quality control and assurance

The laboratory dust generation processes and SEM-EDX analyses were conducted under consistent operating conditions for all samples, using an accelerating voltage of 20 kV and a working distance of $\sim 8 \text{ mm}$ in the Analysis mode. Only particles

with diameters larger than 0.2 μm were measured for size distribution and particle classification due to the 0.2 μm pore size of the sampling filters. The accuracy of the particle size measurements was confirmed using standard polystyrene latex spheres (802 nm \pm 6 nm, Duke Scientific Corp.) under identical CCSEM conditions. The mean size from three independent measurements (each with $n > 6000$ particles) was 796 nm \pm 16 nm. Field blanks showed minimal contamination, with fewer than 20 particles detected per filter. Elemental composition was quantified based on the characteristic X-ray peak intensities, covering elements from carbon (C) to lead (Pb). The EDX software converted these intensities into relative atomic percentages using a ZAF correction procedure (accounting for atomic number, absorption, and fluorescence effects). A quantification threshold of 0.5 wt% and an error margin of 0.1 wt% were applied in the semi-quantitative analysis of elemental contents for particle classification. The mineralogical categorization in this study was determined by comparing the elemental composition of individual particles to the key elements in the empirical formulas of reference minerals. However, since natural particles often exhibit potential impurities, amorphous phases, or solid solutions, those classified under category X are more precisely termed X-like particles to reflect their non-ideal match to the reference mineral. Moreover, aggregated particles with their elemental compositions deviated largely from the formulas were classified into the ‘Mixed silicate minerals’ or ‘Mixed aluminosilicate minerals’ groups.

The detection precision of CCSEM for Si- and Ca-containing particles was evaluated through repeat measurements of two laboratory-generated mineral dust samples from the Taklimakan Desert (sand dune surface soil and gravel soil). Under consistent resuspension and microanalysis conditions, measurements were performed in triplicate on both identical and separate fields of view. Analysis of 11,000 particles per measurement confirmed reproducible detection rates for both particle types (Table S3). The total particle mass derived from CCSEM was compared with that measured by the gravimetric method (Table S4), showing the cumulative uncertainty arising from the ellipsoid volume assumption, the inference of density from composition, and the semi-quantitative nature of EDX analysis. Procedural blanks were measured for gobi and sand sample to quantitatively represent procedural contamination levels in this method (Table S5). To examine the dissolution time series, a separate dust sample from the Taklimakan desert (whose Ca-containing particle abundance fell within the range of the four main samples) underwent double-dialysis. As presented in Table S6, the differences in the number fractions of Ca-containing particles between dialysis cycles were within the pre-dialysis standard deviations for this particle group, indicating that the water-soluble Ca components are effectively removed during a single 2-hour dialysis process. Moreover, an additional acid dialysis experiment at pH = 5.1 \pm 0.1 was performed on the aforementioned sample. The removal of more Ca-containing particles (Table S6) indicated that our relative neutral-water experiment represents a conservative-removal scenario.

210 **3 Results and Discussions**

3.1 Emission fluxes of soluble Ca-containing particles

The total numbers of dust particle decreased slightly across all samples: by 2.8 % and 3.8 % for dust from sandy and gravel surfaces in the Taklimakan Desert, and by 4.7 % and 4.0 % for sandy and gravel dust in the Gobi deserts, respectively. Notably,

after dialysis, the calcium signal disappeared in more than half of the initially Ca-containing particles. This greater decline in
 215 Ca-containing group compared to the total particle count suggests that the vanished particles were mixed-phase, comprising
 water-soluble Ca compounds associated with insoluble minerals. The dialysis process selectively dissolved the soluble Ca
 components from these particles, leaving behind insoluble residues.

Dust aerosols released from gravel surfaces in both deserts contained fewer particles with insoluble Ca components compared
 to those from sandy surfaces. While the proportion of particles containing water-soluble calcium from sandy surfaces ranged
 220 from 56.9 % in the Taklimakan Desert to 80.1 % in the Gobi deserts, gravel surfaces released even higher percentages of such
 particles, including 88.2 % and 85.8 % in the Taklimakan and Gobi deserts, respectively (Fig. 1a). After the removal of water-
 soluble calcium, the remaining insoluble Ca-containing particles exhibited a lower average mass per particle. Nevertheless,
 the mass of individual Ca-containing particles still spanned 4–5 orders of magnitude (Fig. 1b), indicating distinct mineralogical
 compositions between water-soluble calcium compounds and insoluble calcium residues. This interpretation is further
 225 supported by particle volume analysis, which revealed a slight reduction in average volume after dialysis, along with a
 markedly narrower distribution of single-particle volumes in both desert regions (Fig. 1c).

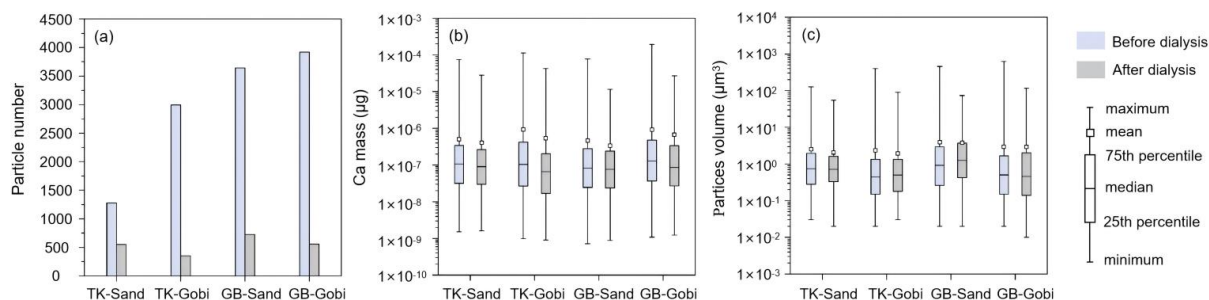


Figure 1. Comparison of total and insoluble Ca-containing single particles before and after water dialysis. (a) Number of Ca-
 230 **containing particles; (b) Mass of elemental Ca per particle (μg); (c) Volume of Ca-containing particles (μm^3).**

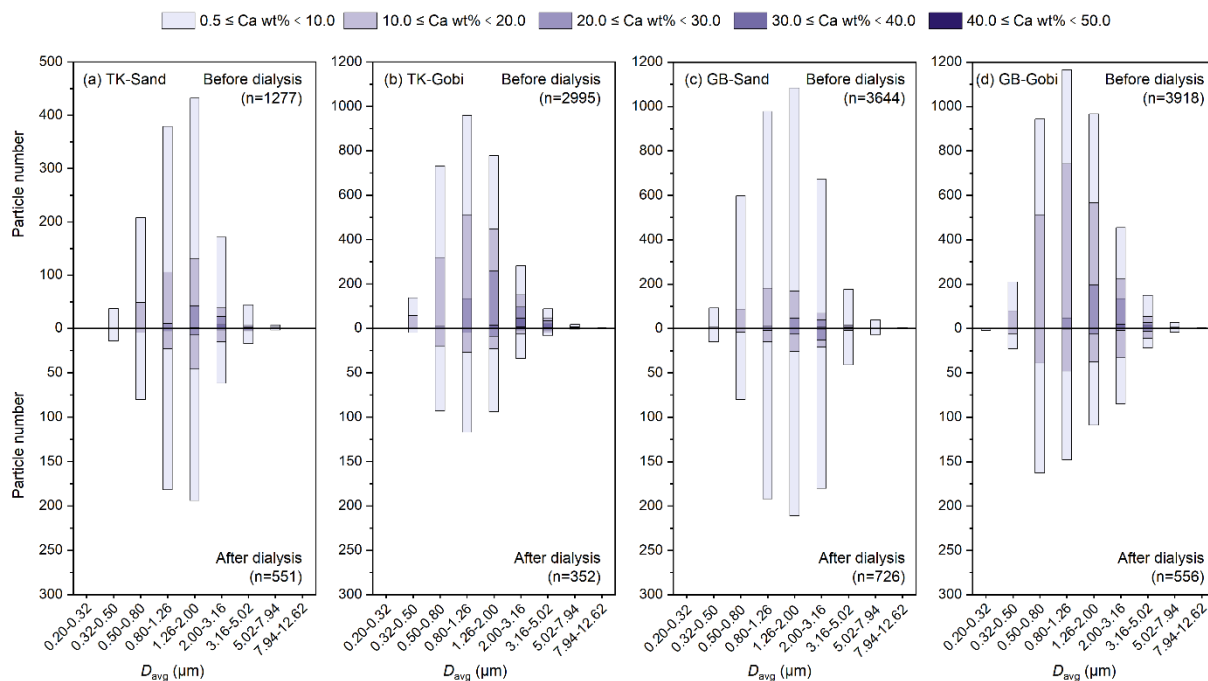
The emission fluxes of Ca-containing particles (Table 1) were estimated based on the measured number concentrations and
 elemental composition of mineral dust particles, combined with the dust generation operating conditions and aerosol sampling
 parameters. A friction velocity of 0.54 m s^{-1} was used to simulate dust mobilization from surface soil via the saltation-
 sandblasting mechanism. By considering the bottom area of the resuspension chamber and the exhaust airflow rate, the
 235 estimated emission fluxes of dust particles containing water-soluble Ca reached average values of $5.0 \times 10^5 \text{ particles m}^{-2} \text{ s}^{-1}$ for
 the Taklimakan Desert and $3.6 \times 10^6 \text{ particles m}^{-2} \text{ s}^{-1}$ for the Gobi deserts. These values account for 9.9 % and 29.2 % of the
 total dust particle number fluxes in each desert, respectively. In mass terms, these water-soluble elemental Ca accounted for
 19.6–41.9 % of the mass of elemental Ca in both the Taklimakan and Gobi deserts. The average fluxes of water-soluble
 240 elemental Ca were $0.4 \mu\text{g m}^{-2} \text{ s}^{-1}$ for the Taklimakan Desert and $3.2 \mu\text{g m}^{-2} \text{ s}^{-1}$ for the Gobi deserts, representing 1.1 % and
 3.3 % of the total dust particle mass fluxes in the Taklimakan and Gobi deserts, respectively. This range is consistent with the

previously reported calcium ion contents of 0.64–5.0 % in both generated dust and ambient dust in the Taklimakan Desert (Wu et al., 2022).

245 **Table 1. Number and mass emission fluxes of total mineral dust and of water-soluble calcium-containing particles/components generated via saltation-sandblasting processes.**

	the Taklimakan Desert			the Gobi deserts		
	Sand dune	Gravel soil	Mean	Sand dune	Gravel soil	Mean
Total dust particles						
Number flux ($\times 10^6$ particles $m^{-2} s^{-1}$)	7.6	2.4	5.0	3.4	21.0	12.2
Mass flux ($\mu g m^{-2} s^{-1}$)	56.4	16.6	36.5	28.6	165.6	97.1
Water-soluble Ca-containing particles/components						
Number flux ($\times 10^5$ particles $m^{-2} s^{-1}$)	4.3	5.6	5.0	8.5	63.0	35.8
Mass flux ($\mu g m^{-2} s^{-1}$)	0.2	0.6	0.4	0.4	6.0	3.2

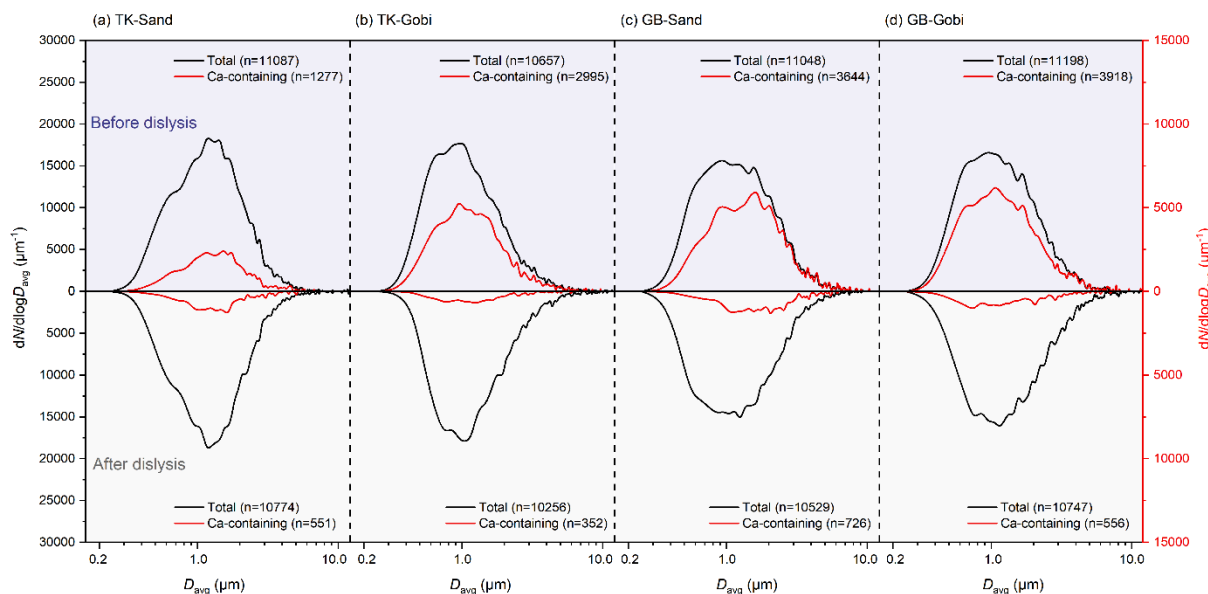
Analysis of individual particles suggests an obvious mineralogical difference between water-soluble and insoluble Ca phases (Fig. 2). Particles with soluble Ca were concentrated in two types with the highest (40.0–50.0 wt %) and lowest (0.5–20.0 wt %) Ca content. The removal of these extreme-composition particles during dialysis, despite unchanged particle size mode, suggests the potential presence of both pure Ca minerals (high-Ca wt % group) and water-soluble Ca-compound coatings (low-Ca group) on the surface of other silicate or aluminosilicate minerals.



255 **Figure 2. Relationship between particle size (μm) and calcium content (relative weight percentage in single particle, Ca wt %) for Ca-bearing particles before and after water dialysis.**

3.2 Physicochemical properties of calcium particles

260 While the size distributions (Fig. 3), elongation (Fig. S4), and roundness (Fig. S5) of both Ca-containing and total dust particles showed little change after dialysis, their surface roughness altered slightly upon removal of water-soluble Ca compounds (Fig. S6). The development of more irregular particle edges confirms that the dissolved components had previously formed uniform coatings over the inherently rougher surfaces of the insoluble mineral cores.



265 **Figure 3. Particle number size distributions of Ca-containing and total dust particles generated from sandy (Sand) and gravel (Gobi) surface soils of the Taklimakan (TK) and Gobi (GB) Desert.**

To further characterize the dissolution behavior of different minerals and their mixing states, individual Ca-containing dust particles were categorized into several mineralogical subgroups according to their empirical formula: clay mineral-like (e.g. smectite and vermiculite), feldspar-like (e.g. anorthite and albite), calcite-like, dolomite-like, gypsum-like, and others (comprising mixed silicates or aluminosilicates with elemental compositions not matching any specific mineral). The relative abundances of each mineral varied across deserts and surface soil types (Fig. 4). Post-dialysis, the lowest residual fractions of Ca-containing minerals were observed for calcite-like (ranging from 0.1 % to 0.7 % in total dust particles from the Taklimakan and Gobi deserts) and gypsum-like (0.0 % in all samples) groups, suggesting them as the most soluble minerals.

275

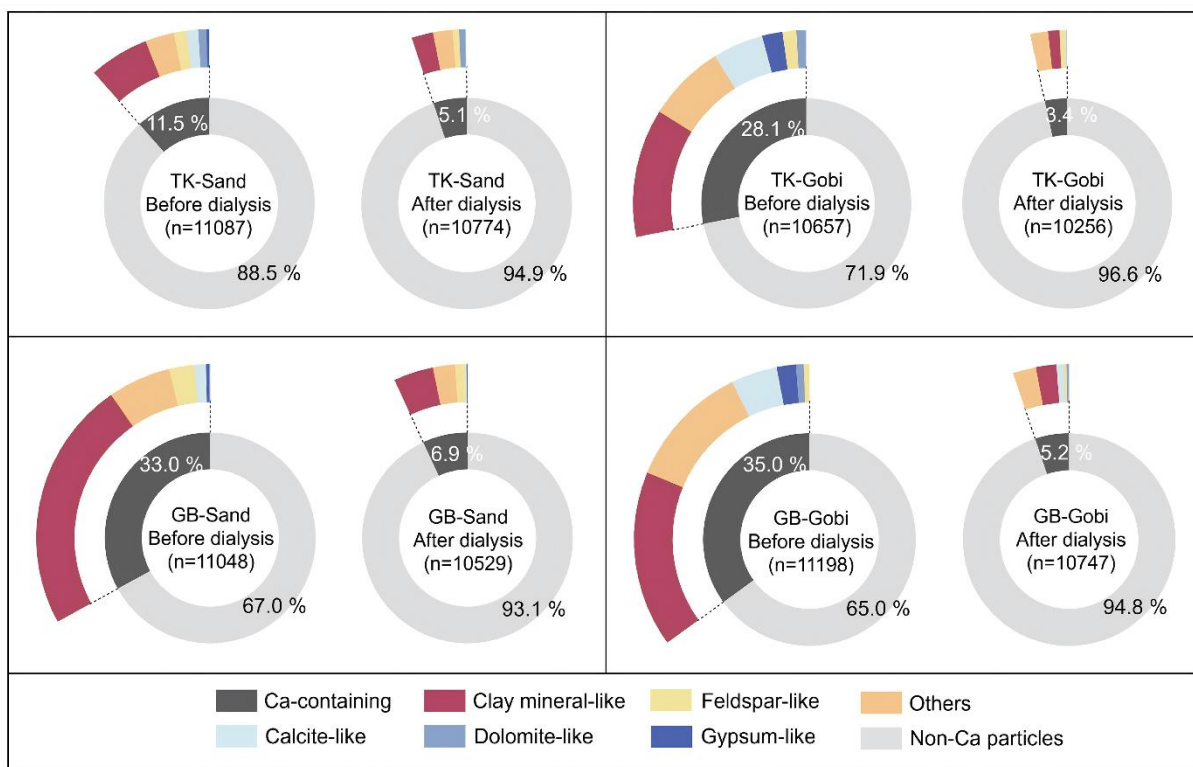
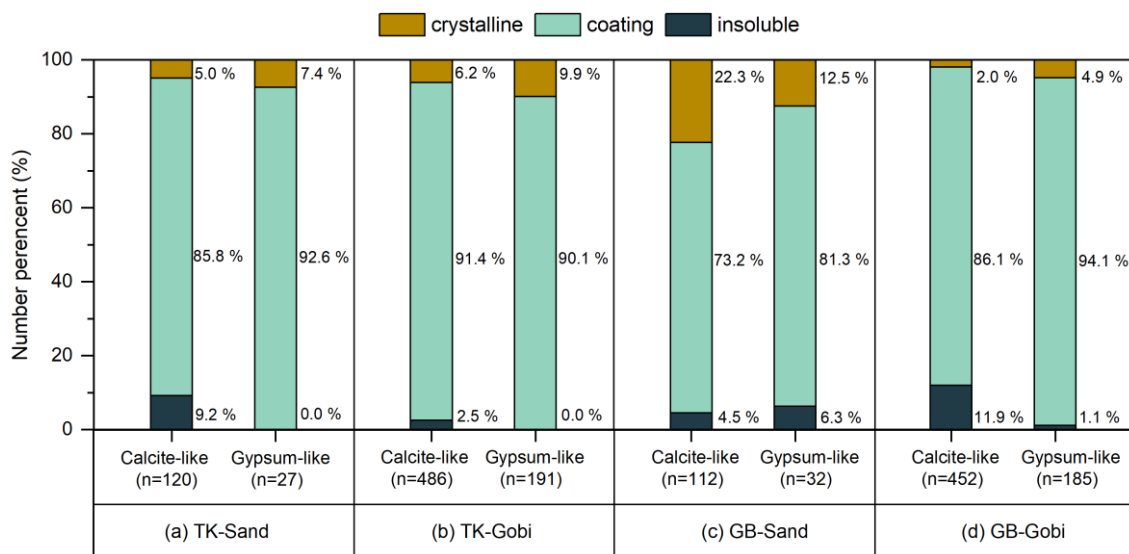


Figure 4. Relative number abundances of Ca-containing minerals before and after water dialysis. Dust samples were generated from sandy (Sand) and gravel (Gobi) surface soils of the Taklimakan (TK) and the Gobi (GB) Desert.

280 To this end, we performed targeted manual EDX mapping on individual Ca-O-rich and Ca-S-containing particles to
supplementally assess changes in their mixing states. Most Ca-O-rich (calcite-like) particles exhibited minimal morphological
change following dialysis. These were inferred to be Ca-O-rich components internally mixed with other minerals (i.e., coating
on) other minerals. Their proportion varied geographically, accounting for 73.2 % of Ca-O-rich particles from sandy Gobi
desert surfaces to 91.4 % from gravel surfaces in the Taklimakan Desert (Fig. 5). The proportion of dust particles containing
285 a Ca-S-containing (gypsum-like) coating was even higher, exceeding 81.3 % across all samples. In contrast, particles that
vanished during dialysis were categorized as a crystalline group, likely consisting of relatively pure mineral phases.



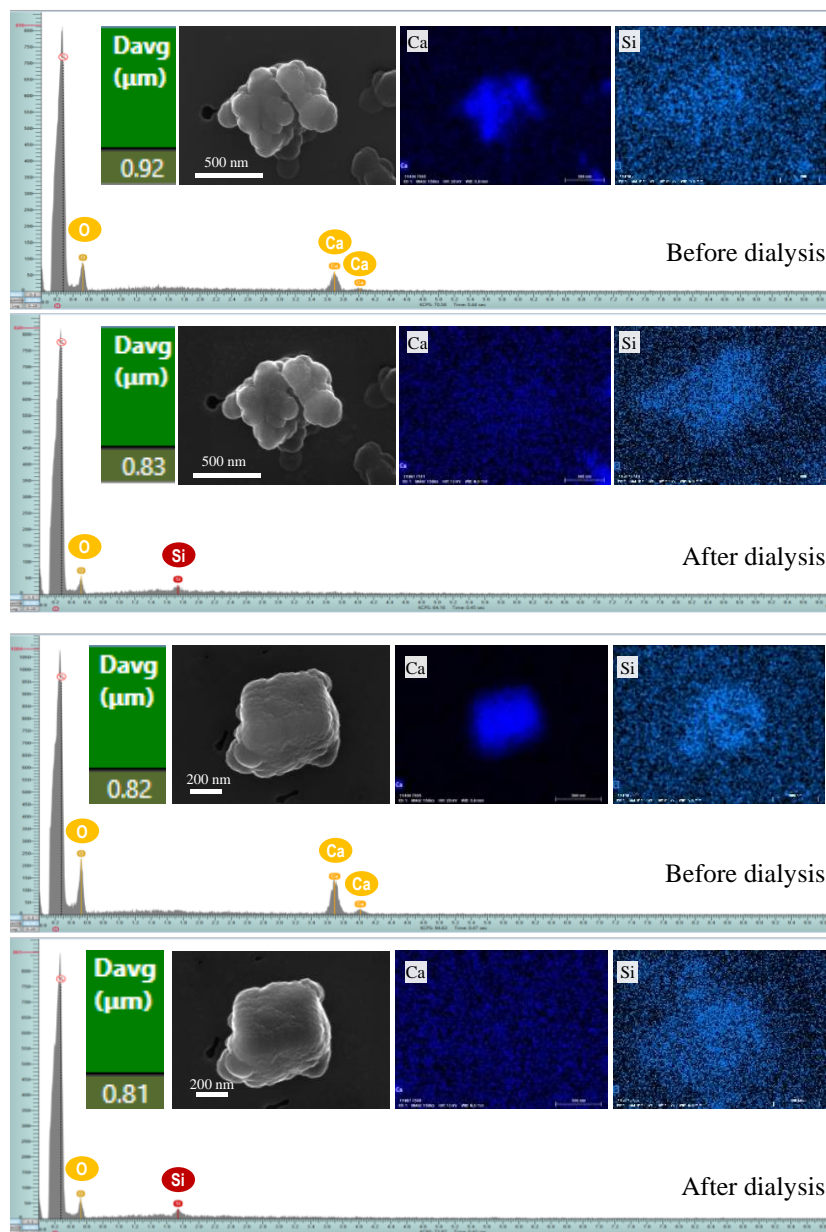
290 **Figure 5. Relative particle number percentage of Ca-O-rich (calcite-like) and Ca-S-containing (gypsum-like) particles in different mixing states. The numbers in the parentheses are the counts of detected Ca-O-rich and Ca-S-containing particles.**

3.3 Rapid buffering of soluble calcium components

The morphology of dust particles coated with Ca-O-rich (Fig. 6) and Ca-S-containing (Fig. S7) material is presented together with their corresponding EDX point spectra (taken at the point computed to be most distant from the particle edge) and elemental distribution mappings (over the projected particle area) across the dialysis process. A multi-part chain of evidence confirms the presence of water-soluble Ca-rich coatings on insoluble mineral dust particles. First, both EDX spectra and elemental mappings show the disappearance of the Ca signal after dialysis, indicating the removal of a Ca-rich phase. Second, SEM micrographs reveal that particle morphology remains essentially unchanged after dialysis, while a subtle but measurable decrease in diameter occurs. This pattern is consistent with the loss of a thin surface layer rather than with bulk dissolution of the core. Third, post-dialysis EDX spectra display newly-appeared peaks of Si (and frequently Al), elements characteristic of the underlying insoluble silicate or aluminosilicate core. This further confirms that removal of the surface Ca-coatings exposes the persistent mineral substrate. Based on the projected outlines in high-resolution micrographs, the thickness of the Ca-O-rich and Ca-S-containing coatings is estimated to be on the order of 10–100 nm.

295

300



305

Figure 6. Micrographs of typical Ca-O particles and their EDX elemental mappings / spectra illustrate the coating of water-soluble Ca-O-rich components on the surface of Si-containing particles. The EDX spectrum shows the elemental composition at the point to be most distant from the particle edge, while the EDX mapping displays the distribution of elements within its projected area.

310 The atmospheric importance of such a thin, water-soluble Ca-rich coating on an insoluble mineral core lies in its capacity to neutralize acidic gases, thereby exerting a buffering effect on aerosol chemistry. Ca-rich minerals (e.g., calcite) are ubiquitous in arid and semi-arid surface soils and constitute a substantial fraction of globally emitted alkaline dust. During atmospheric

transport, calcite acts as an effective alkaline agent, neutralizing acids such as H_2SO_4 , HNO_3 , and SO_2 (Wang Y. et al., 2012). Calcite dissolution has been identified as a surface-controlled process (Laanait et al., 2015), thus its kinetics are largely
315 influenced by mass-transport limitations, underscoring the importance of particle size and mixing state (Batchelor-McAuley et al., 2022). Nevertheless, key constraints such as reaction timescales and size-dependent effects are often oversimplified or entirely omitted in global models, where dust particles are typically assumed to undergo either instantaneous complete dissolution or equilibrium partitioning (Pye et al., 2020). Our automated microanalysis shows that 56.9–88.2% of Ca-containing dust particles released their water-soluble Ca components. We further infer that the Ca-O-rich component, most
320 likely calcite, one of the most soluble minerals in the source dust, exists predominantly as 10–100 nm-thick coatings on micron- and submicron-sized insoluble particles. This specific mixing state may accelerate the dissolution kinetics of calcite by altering the mass-transfer rate. These findings provide observational constraints on water-soluble Ca associated with fine dust particles from two Asian deserts and offer qualitative insights, from a single-particle perspective, into the physicochemical properties of freshly emitted mineral dust.

325 Moreover, our dialysis experiment was designed to examine the abundance and mixing state of water-soluble Ca components on dust particles, not to simulate atmospheric cloud processing. Dialysis in Milli-Q water (pre-equilibrated in open air at 25 ± 5 °C for 48 hours, $\text{pH } 6.4 \pm 0.7$) effectively removed soluble material, and subsequent CCSEM analysis quantified the resulting changes in surface composition. In contrast, a separate humidity-exposure experiment (Fig. S8) demonstrated that under thin-film conditions, more representative of atmospheric moisture, these coatings dissolved and recrystallized upon drying rather
330 than being fully removed (Fig. S9 and S10). This implies that our dialysis setup, employing bulk water at near-neutral pH, likely yields a conservative estimate of coating removal, given that atmospheric waters are often acidic and contain ions that could enhance dissolution. In model simulations, calcite is often treated as a sparingly soluble mineral whose dissolution is kinetically controlled and highly dependent on ambient acidity (pH). An additional acid dialysis performed on a separate dust sample after dual water dialysis (Table S6) confirmed that acidic conditions promote the dissolution of Ca-containing particles.

335 Although not a direct replication of in-cloud conditions, this study clearly establishes the presence of water-soluble calcium coatings on dust particles, a feature relevant to climate-related properties such as cloud-condensation activity.

3.4 Strengths and limitations of the experimental approach

The limited number of geographic sampling sites in this work is compensated for by the identical dust-generating conditions
340 and high statistical robustness achieved at the particle-population level. During sampling with the suspension chamber, two measures were employed to reduce artifacts: the use of conductive silicone rubber tubing and the application of chemical and static passivation to all interior aluminum surfaces. Furthermore, CCSEM-derived particle masses on polycarbonate substrates were calibrated via a gravimetric method using simultaneous collections on quartz filters (Table S4). And procedural blanks were used to assess and correct for contamination. However, this study did not quantify particle losses in the sampling line or

345 the subsequent propagation of measurement uncertainty. Therefore, the absolute flux values presented here remain order-of-magnitude estimates.

The automated microanalysis via CCSEM allowed for the precise relocation of all previously analyzed fields of view and the subsequent measurement of all residual particles within these areas post-dialysis. This process allowed quantification of the size distribution and elemental composition of the same set of dust particles on a single-particle basis, with each sample
350 containing over 10,000 particles. By applying the identical CCSEM operating conditions used prior to dialysis, the number of water-soluble Ca-containing particles and the mass of soluble Ca were estimated based on several assumptions regarding particle shape and density. However, these assumptions, such as regarding particles as ellipsoids and assigning densities based on elemental composition, may introduce uncertainties due to the inherent physicochemical complexity of mineral dust particles in environmental samples.

355 It is also important to note a key limitation of the EDX-based CCSEM technique: its inability to determine chemical bonding. Consequently, the identification of calcium carbonate (CaCO_3) solely based on the detection of Ca–O-rich particles, where the combined weight percentage of Ca and O exceeds 99.0 wt %, is subject to uncertainty. This approach cannot exclude the potential presence of other Ca–O-rich phases such as calcium oxide (CaO), calcium hydroxide (Ca(OH)_2), and calcium nitrate ($\text{Ca(NO}_3)_2$), all of which exhibit EDX spectra similar to that of CaCO_3 . It is worth noting, however, that CaO tends to react
360 with atmospheric moisture, forming Ca(OH)_2 , which can further react with CO_2 to yield amorphous calcium carbonate (Barker, 1974; Kalinkin et al., 2005). In addition, $\text{Ca(NO}_3)_2$ is not commonly observed as a typical mineral in dust samples from source regions, as indicated by bulk measurements of calcium and nitrate among water-soluble ions (Wu et al., 2022) and downwind individual particle analysis (Laskin et al., 2005). Under these considerations, calcite is generally regarded as the most probable source mineral (Fitzgerald et al., 2015; Panta et al., 2022).

365 Finally, the current methodology remains time-intensive, requiring tens of hours per sample for the relocation of Ca-O-rich and Ca-S-containing particles and the visual identification of their mixing states. Consequently, only four samples were analyzed, which precludes any meaningful assessment of standard deviation across individual environmental samples.

4 Summary and Implications

Mineral dust from arid and semi-arid regions is one of the most abundant atmospheric aerosols by mass. Its substantial chemical
370 evolution during transport profoundly influences the climate system. This study provides a quantitative, single-particle constraint, showing that water-soluble calcium constitutes 56.9–88.2 % (by number) in dust aerosols from two Asian deserts. Importantly, over 73 % of this calcium exists as surface coatings, making it readily available for rapid dissolution even under moderately acidic conditions. This rapid dissolution likely enhances the acid-neutralizing capacity of freshly emitted dust from saltation-sandblasting processes. Therefore, accurately projecting the role of dust in the Earth system requires that future
375 experimental and modelling frameworks explicitly account for its transport, chemical evolution, and the mass balance of alkalinity delivery.

Data availability

All data supporting this study are available in the main 920 text and its supplementary materials. Additionally, the datasets (Physicochemical Properties of Water-Dialyzed Single Asian Dust Particles) have been permanently archived in the Mendeley
380 Data repository ([https://doi.org/ 10.17632/4js9dfy9hm.1](https://doi.org/10.17632/4js9dfy9hm.1)).

Author contribution

JC and DZ designed the experiments and TH carried them out. TH, DZ, and YS developed the methodology and YS performed the individual particle analysis. TH, NJ, and YS prepared the manuscript with contributions from all co-authors.

Competing interests

385 The authors declare that they have no conflict of interest.

Financial support

This study was supported by the National Natural Science Foundation of China (42030511).

References

- Adebisi, A., Kok, J. F., Murray, B. J., Ryder, C. L., Stuu, J.-B. W., Kahn, R. A., Knippertz, P., Formenti, P., Mahowald, N.
390 M., Pérez García-Pando, C., Klose, M., Ansmann, A., Samset, B. H., Ito, A., Balkanski, Y., Di Biagio, C., Romanias, M.
N., Huang, Y., and Meng, J.: A review of coarse mineral dust in the Earth system, *Aeolian Res.*, 60, 100849,
<https://doi.org/10.1016/j.aeolia.2022.100849>, 2023.
- Alfaro, S., Bouet, C., Khalfallah, B., Shao, Y., Ishizuka, M., Labiadh, M., Marticorena, B., Laurent, B., and Rajot, J. L.:
Unraveling the roles of saltation bombardment and atmospheric instability on magnitude and size distribution of dust
395 emission fluxes: Lessons from the JADE and WIND - O - V experiments, *J. Geophys. Res. Atmos.*, 127,
e2021JD035983, <https://doi.org/10.1029/2021JD035983>, 2022.
- Alfaro, S. C.: Influence of soil texture on the binding energies of fine mineral dust particles potentially released by wind
erosion, *Geomorphology*, 93, 157-167, <https://doi.org/10.1016/j.geomorph.2007.02.012>, 2008.
- Alfaro, S. C., Gaudichet, A., Gomes, L., and Maillé M.: Modeling the size distribution of a soil aerosol produced by
400 sandblasting, *J. Geophys. Res. Atmos.*, 102, 11239-11249, <https://doi.org/10.1029/97JD00403>, 1997.
- ASTM International: Standard practice for characterization of particles, ASTM F1877-16, <https://doi.org/10.1520/F1877-16>
(last access: 20 November 2025), 2016.

- Ault, A. P., Peters, T. M., Sawvel, E. J., Casuccio, G. S., Willis, R. D., Norris, G. A., and Grassian, V. H.: Single-particle SEM-EDX analysis of iron-containing coarse particulate matter in an urban environment: sources and distribution of iron within Cleveland, Ohio, *Environ. Sci. Technol.*, 46, 4331-4339, <https://doi.org/10.1021/es204006k>, 2012.
- 405 Barker, R., The reactivity of calcium oxide towards carbon dioxide and its use for energy storage, *J. Appl. Chem. Biotechnol.*, 24, 221-227, <https://doi.org/10.1002/jctb.5020240405>, 1974.
- Batchelor-McAuley, C., Yang, M., Rickaby, R. E., and Compton, R. G.: Calcium carbonate dissolution from the laboratory to the ocean: Kinetics and mechanism, *Chem. Eur. J.*, 28, e202202290, <https://doi.org/10.1002/chem.202202290>, 2022.
- 410 Cao, J. J., Lee, S. C., Zhang, X. Y., Chow, J. C., An, Z. S., Ho, K. F., Watson, J. G., Fung, K., Wang, Y. Q., and Shen, Z. X.: Characterization of airborne carbonate over a site near Asian dust source regions during spring 2002 and its climatic and environmental significance, *J. Geophys. Res. Atmos.*, 110, <https://doi.org/10.1029/2004JD005244>, 2005.
- Carter, B. R., Toggweiler, J. R., Key, R. M., and Sarmiento, J. L.: Processes determining the marine alkalinity and calcium carbonate saturation state distributions, *Biogeosciences*, 11, 7349-7362, <https://doi.org/10.5194/bg-11-7349-2014>, 2014,
- 415 2014.
- Castillo, M. D., Wagner, J., Casuccio, G. S., West, R. R., Freedman, F. R., Eisl, H. M., Wang, Z.-M., Yip, J. P., and Kinney, P. L.: Field testing a low-cost passive aerosol sampler for long-term measurement of ambient PM_{2.5} concentrations and particle composition, *Atmos. Environ.*, 216, 116905, <https://doi.org/10.1016/j.atmosenv.2019.116905>, 2019.
- Choobari, O. A., Zawar-Reza, P., and Sturman, A.: The global distribution of mineral dust and its impacts on the climate system: A review, *Atmos. Res.*, 138, 152-165, <https://doi.org/10.1016/j.atmosres.2013.11.007>, 2014.
- 420 Cook, R. B.: *Handbook of mineralogy, Rocks Miner.*, 76: 278, 2001.
- Craig, R. L., and Ault, A. P.: Aerosol acidity: direct measurement from a spectroscopic method, in: *Multiphase Environmental Chemistry in the Atmosphere*, edited by: Pratt, K. A., and Farmer, D. K., American Chemical Society, Washington, DC, USA, 171–191, <https://doi.org/10.1021/bk-2018-1299.ch009>, 2018
- 425 Craig, R. L., Peterson, P. K., Nandy, L., Lei, Z., Hossain, M. A., Camarena, S., Dodson, R. A., Cook, R. D., Dutcher, C. S., and Ault, A. P.: Direct determination of aerosol pH: Size-resolved measurements of submicrometer and supermicrometer aqueous particles, *Anal. Chem.*, 90, 11232-11239, <https://doi.org/10.1021/acs.analchem.8b00586>, 2018.
- Declat, A., Reyes, E., and Suárez, O. M.: Calcium carbonate precipitation: a review of the carbonate crystallization process and applications in bioinspired composites, *Reviews on Adv. Mater. Sci.*, 44, 87–107, 2016.
- 430 El-Baz, F.: *Desert and Arid Lands*, Springer, Dordrecht, Netherlands, 222 pp., <https://doi.org/10.1007/978-94-009-6080-0>, 2012.
- Engelbrecht, J. P., and Derbyshire, E.: Airborne mineral dust, *Elements*, 6, 241-246, <http://dx.doi.org/10.2113/gselements.6.4.241>, 2010.
- Falkovich, A. H., Ganor, E., Levin, Z., Formenti, P., and Rudich, Y.: Chemical and mineralogical analysis of individual mineral dust particles, *J. Geophys. Res. Atmos.*, 106, 18029-18036, <https://doi.org/10.1029/2000JD900430>, 2001.
- 435

- Fantle, M. S., and Tipper, E. T.: Calcium isotopes in the global biogeochemical Ca cycle: Implications for development of a Ca isotope proxy, *Earth-Sci. Rev.*, 129, 148-177, <https://doi.org/10.1016/j.earscirev.2013.10.004>, 2014.
- 440 Feely, R. A., Sabine, C. L., Lee, K., Millero, F. J., Lamb, M. F., Greeley, D., Bullister, J. L., Key, R. M., Peng, T.-H., Kozyr, A., Ono, T., and Wong, C. S.: In situ calcium carbonate dissolution in the Pacific Ocean, *Glob. Biogeochem. Cycles*, 16, 91-91-91-12, <https://doi.org/10.1029/2002GB001866>, 2002.
- Fitzgerald, E., Ault, A. P., Zauscher, M. D., Mayol-Bracero, O. L., and Prather, K. A.: Comparison of the mixing state of long-range transported Asian and African mineral dust, *Atmos. Environ.*, 115, 19-25, <https://doi.org/10.1016/j.atmosenv.2015.04.031>, 2015.
- 445 Formenti, P., Schütz, L., Balkanski, Y., Desboeufs, K., Ebert, M., Kandler, K., Petzold, A., Scheuven, D., Weinbruch, S., and Zhang, D.: Recent progress in understanding physical and chemical properties of African and Asian mineral dust, *Atmos. Chem. Phys.*, 11, 8231-8256, <https://doi.org/10.5194/acp-11-8231-2011>, 2011.
- Grini, A., and Zender, C. S.: Roles of saltation, sandblasting, and wind speed variability on mineral dust aerosol size distribution during the Puerto Rican Dust Experiment (PRIDE), *J. Geophys. Res. Atmos.*, 109, <https://doi.org/10.1029/2003JD004233>, 2004.
- 450 Grini, A., Zender, C. S., and Colarco, P. R.: Saltation Sandblasting behavior during mineral dust aerosol production, *Geophys. Res. Lett.*, 29, 15-11-15-14, <https://doi.org/10.1029/2002GL015248>, 2002.
- Guo, L., Gu, W., Peng, C., Wang, W., Li, Y. J., Zong, T., Tang, Y., Wu, Z., Lin, Q., Ge, M., Zhang, G., Hu, M., Bi, X., Wang, X., and Tang, M.: A comprehensive study of hygroscopic properties of calcium- and magnesium-containing salts: implication for hygroscopicity of mineral dust and sea salt aerosols, *Atmos. Chem. Phys.*, 19, 2115-2133, <https://doi.org/10.5194/acp-19-2115-2019>, 2019.
- 455 Gussone, N., Schmitt, A. D., Heuser, A., Wombacher, F., Dietzel, M., Tipper, E., and Schiller, M.: Calcium stable isotope geochemistry, *Advances in Isotope Geochemistry*, Springer, Berlin, Heidelberg, Germany, 260 pp., <https://doi.org/10.1007/978-3-540-68953-9>, 2016.
- Jickells, T., Boyd, P., and Hunter, K. A.: Biogeochemical Impacts of Dust on the Global Carbon Cycle, in: *Mineral Dust: A key player in the Earth system*, edited by: Knippertz, P., and Stuut, J. B. W., Springer, Dordrecht, Netherlands, 359-384, https://doi.org/10.1007/978-94-017-8978-3_14, 2014.
- 460 Kalinkin, A. M., Kalinkina, E. V., Zalkind, O. A., and Makarova, T. I.: Chemical interaction of calcium oxide and calcium hydroxide with CO₂ during mechanical activation, *Inorg. Mater.*, 41, 1073-1079, <https://doi.org/10.1007/s10789-005-0263-1>, 2005.
- 465 Kandler, K., Lieke, K., Benker, N., Emmel, C., Küpper, M., Müller-Ebert, D., Ebert, M., Scheuven, D., Schladitz, A., Schütz, L., and Weinbruch, S.: Electron microscopy of particles collected at Praia, Cape Verde, during the Saharan Mineral Dust Experiment: particle chemistry, shape, mixing state and complex refractive index, *Tellus B: Chem. Phys. Meteorol.*, 63, 475-496, <https://doi.org/10.1111/j.1600-0889.2011.00550.x>, 2011.

- Knippertz, P., and Stuut, J. B. W. (Eds.): Mineral dust: A key player in the Earth system, Springer, Dordrecht, Netherlands, 509 pp., <https://doi.org/10.1007/978-94-017-8978-3>, 2014.
- 470 Kok, J. F., Adebisi, A. A., Albani, S., Balkanski, Y., Checa-Garcia, R., Chin, M., Colarco, P. R., Hamilton, D. S., Huang, Y., Ito, A., Klose, M., Leung, D. M., Li, L., Mahowald, N. M., Miller, R. L., Obiso, V., Pérez García-Pando, C., Rocha-Lima, A., Wan, J. S., and Whicker, C. A.: Improved representation of the global dust cycle using observational constraints on dust properties and abundance, *Atmos. Chem. Phys.*, 21, 8127-8167, <https://doi.org/10.5194/acp-21-8127-2021>, 2021a.
- 475 Kok, J. F., Adebisi, A. A., Albani, S., Balkanski, Y., Checa-Garcia, R., Chin, M., Colarco, P. R., Hamilton, D. S., Huang, Y., Ito, A., Klose, M., Li, L., Mahowald, N. M., Miller, R. L., Obiso, V., Pérez García-Pando, C., Rocha-Lima, A., and Wan, J. S.: Contribution of the world's main dust source regions to the global cycle of desert dust, *Atmos. Chem. Phys.*, 21, 8169–8193, <https://doi.org/10.5194/acp-21-8169-2021>, 2021b.
- Kok, J. F., Storelvmo, T., Karydis, V. A., Adebisi, A. A., Mahowald, N. M., Evan, A. T., He, C., and Leung, D. M.: Mineral dust aerosol impacts on global climate and climate change. *Nature Reviews Earth & Environment*, 4(2), 71-86, <https://doi.org/10.1038/s43017-022-00379-5>, 2023.
- 480 Krueger, B. J., Grassian, V. H., Cowin, J. P., and Laskin, A.: Heterogeneous chemistry of individual mineral dust particles from different dust source regions: the importance of particle mineralogy, *Atmos. Environ.*, 38, 6253-6261, <https://doi.org/10.1016/j.atmosenv.2004.07.010>, 2004.
- 485 Krueger, B. J., Grassian, V. H., Laskin, A., and Cowin, J. P.: The transformation of solid atmospheric particles into liquid droplets through heterogeneous chemistry: Laboratory insights into the processing of calcium containing mineral dust aerosol in the troposphere, *Geophys. Res. Lett.*, 30, <https://doi.org/10.1029/2002GL016563>, 2003.
- Laanait, N., Callagon, E. B. R., Zhang, Z., Sturchio, N. C., Lee, S. S., and Fenter, P.: X-ray-driven reaction front dynamics at calcite-water interfaces, *Science*, 349, 1330-1334, <https://doi.org/10.1126/science.aab3272>, 2015.
- 490 Laskin, A., Iedema, M. J., Ichkovich, A., Graber, E. R., Taraniuk, I., and Rudich, Y.: Direct observation of completely processed calcium carbonate dust particles, *Farad. Discuss.*, 130, 453-468, <https://doi.org/10.1039/B417366J>, 2005.
- Laurent, B., Marticorena, B., Bergametti, G., Chazette, P., Maignan, F., Schmechtig, C.: Simulation of the mineral dust emission frequencies from desert area of China and Mongolia using an aerodynamic roughness length map derived from the POLDER/ADEOS surface products. *J. Geophys. Res.* 110, D18S04. <https://doi.org/10.1029/2004JD005013>, 2005.
- 495 Maher, B. A., Prospero, J. M., Mackie, D., Gaiero, D., Hesse, P. P., and Balkanski, Y.: Global connections between aeolian dust, climate and ocean biogeochemistry at the present day and at the last glacial maximum, *Earth-Sci. Rev.*, 99, 61-97, <https://doi.org/10.1016/j.earscirev.2009.12.001>, 2010.
- Mahowald, N., Albani, S., Kok, J. F., Engelstaeder, S., Scanza, R., Ward, D. S., and Flanner, M. G.: The size distribution of desert dust aerosols and its impact on the Earth system, *Aeolian Res.*, 15, 53-71, <https://doi.org/10.1016/j.aeolia.2013.09.002>, 2014.
- 500

- Mahowald, N. M., Hamilton, D. S., Mackey, K. R. M., Moore, J. K., Baker, A. R., Scanza, R. A., and Zhang, Y.: Aerosol trace metal leaching and impacts on marine microorganisms, *Nat. Commun.*, 9, 2614, <https://doi.org/10.1038/s41467-018-04970-7>, 2018.
- 505 Mamane, Y., Willis, R., and Conner, T.: Evaluation of computer-controlled scanning electron microscopy applied to an ambient urban aerosol sample, *Aerosol Sci. Technol.*, 34, 97-107, <https://doi.org/10.1080/02786820118842>, 2001.
- Mikami, M., Yamada, Y., Ishizuka, M., Ishimaru, T., Gao, W., and Zeng, F.: Measurement of saltation process over gobi and sand dunes in the Taklimakan desert, China, with newly developed sand particle counter, *J. Geophys. Res. Atmos.*, 110, <https://doi.org/10.1029/2004JD004688>, 2005.
- Morse, J. W., Arvidson, R. S., and Lüttge, A.: Calcium carbonate formation and dissolution, *Chem. Rev.*, 107, 342-381, <https://doi.org/10.1021/cr050358j>, 2007.
- 510 Nousiainen, T.: Optical modeling of mineral dust particles: A review, *J. Quant. Spectrosc. Radiat. Transf.*, 110, 1261-1279, <https://doi.org/10.1016/j.jqsrt.2009.03.002>, 2009.
- Panta, A., Kandler, K., Alastuey, A., González-Flórez, C., González-Romero, A., Klose, M., Querol, X., Reche, C., Yus-Déz, J., and Pérez García-Pando, C.: Insights into the single-particle composition, size, mixing state, and aspect ratio of freshly emitted mineral dust from field measurements in the Moroccan Sahara using electron microscopy, *Atmos. Chem. Phys.*, 23, 3861-3885, <https://doi.org/10.5194/acp-23-3861-2023>, 2023.
- 515 Parajuli, S. P., Zobeck, T. M., Kocurek, G., Yang, Z.-L., and Stenchikov, G. L.: New insights into the wind-dust relationship in sandblasting and direct aerodynamic entrainment from wind tunnel experiments, *J. Geophys. Res. Atmos.*, 121, 1776-1792, <https://doi.org/10.1002/2015JD024424>, 2016.
- 520 Pye, H. O. T., Nenes, A., Alexander, B., Ault, A. P., Barth, M. C., Clegg, S. L., Collett Jr, J. L., Fahey, K. M., Hennigan, C. J., Herrmann, H., Kanakidou, M., Kelly, J. T., Ku, I. T., McNeill, V. F., Riemer, N., Schaefer, T., Shi, G., Tilgner, A., Walker, J. T., Wang, T., Weber, R., Xing, J., Zaveri, R. A., and Zuend, A.: The acidity of atmospheric particles and clouds, *Atmos. Chem. Phys.*, 20, 4809-4888, <https://doi.org/10.5194/acp-20-4809-2020>, 2020.
- Pye, K.: *Aeolian dust and dust deposits*, Elsevier, Amsterdam, Netherlands, <https://doi.org/10.1016/C2013-0-05007-4>, 2015.
- 525 Quigg, A.: Micronutrients, in: *The Physiology of Microalgae, Developments in Applied Phycology*, edited by: Borowitzka, M. A., Beardall, J., and Raven, J. A., Springer, Cham, Switzerland, 211-231, https://doi.org/10.1007/978-3-319-24945-2_10, 2016.
- Ren, L., Wang, W., Wang, Q., Yang, X., and Tang, D.: Comparison and trend study on acidity and acidic buffering capacity of particulate matter in China, *Atmos. Environ.*, 45, 7503-7519, <https://doi.org/10.1016/j.atmosenv.2010.08.055>, 2011.
- 530 Schepanski, K.: Transport of mineral dust and its impact on climate, *Geosciences*, 8, 151, <https://doi.org/10.3390/geosciences8050151>, 2018.
- Shao, Y.: A model for mineral dust emission, *J. Geophys. Res. Atmos.*, 106, 20239-20254, <https://doi.org/10.1029/2001JD900171>, 2001.

- Shao, Y., and Dong, C. H.: A review on East Asian dust storm climate, modelling and monitoring, *Glob. Planet. Change*, 52, 1-22, <https://doi.org/10.1016/j.gloplacha.2006.02.011>, 2006.
- 535
- Shao, Y., Raupach, M. R., and Findlater, P. A.: Effect of saltation bombardment on the entrainment of dust by wind, *J. Geophys. Res. Atmos.*, 98, 12719-12726, <https://doi.org/10.1029/93JD00396>, 1993.
- Singh, O. N. and Fabian, P. (Eds.): *Atmospheric Ozone: a Millennium Issue*, Copernicus Publications, Katlenburg-Lindau, Germany, 147 pp., ISBN 393658608X, 2003.
- 540
- Steiner, Z., Sarkar, A., Liu, X., Berelson, W. M., Adkins, J. F., Achterberg, E. P., Sabu, P., Prakash, S., Vinaychandran, P. N., Byrne, R. H., and Turchyn, A. V.: On calcium-to-alkalinity anomalies in the North Pacific, Red Sea, Indian Ocean and Southern Ocean, *Geochim. Cosmochim. Acta*, 303, 1-14, <https://doi.org/10.1016/j.gca.2021.03.027>, 2021.
- Su, J., Cai, W.-J., Brodeur, J., Chen, B., Hussain, N., Yao, Y., Ni, C., Testa, J. M., Li, M., Xie, X., Ni, W., Scaboo, K. M., Xu, Y.-y., Cornwell, J., Gurbisz, C., Owens, M. S., Waldbusser, G. G., Dai, M., and Kemp, W. M.: Chesapeake Bay acidification buffered by spatially decoupled carbonate mineral cycling, *Nat. Geosci.*, 13, 441-447, <https://doi.org/10.1038/s41561-020-0584-3>, 2020.
- 545
- Sullivan, R. C., Moore, M. J. K., Petters, M. D., Kreidenweis, S. M., Roberts, G. C., and Prather, K. A.: Effect of chemical mixing state on the hygroscopicity and cloud nucleation properties of calcium mineral dust particles, *Atmos. Chem. Phys.*, 9, 3303-3316, <https://doi.org/10.5194/acp-9-3303-2009>, 2009.
- 550
- Sulpis, O., Jeansson, E., Dinauer, A., Lauvset, S. K., and Middelburg, J. J.: Calcium carbonate dissolution patterns in the ocean, *Nat. Geosci.*, 14, 423-428, <https://doi.org/10.1038/s41561-021-00743-y>, 2021.
- Sun, J., and Liu, T.: The age of the Taklimakan Desert, *Science*, 312, 1621-1621, <https://doi.org/10.1126/science.1124616>, 2006.
- Sweeney, M.R., Lu, H., Cui, M., Mason, J.A., Feng, H., Xu, Z.: Sand dunes as potential sources of dust in northern China. *Sci. China Earth Sci.* 59 (4), 760–769. <https://doi.org/10.1007/s11430-015-5246-8>, 2016.
- 555
- Tegen, I., and Fung, I.: Modeling of mineral dust in the atmosphere: Sources, transport, and optical thickness, *J. Geophys. Res. Atmos.*, 99, 22897-22914, <https://doi.org/10.1029/94JD01928>, 1994.
- Tipper, E.T., Schmitt, AD., and Gussone, N.: Global Ca cycles: coupling of continental and oceanic processes, in: *Calcium Stable Isotope Geochemistry, Advances in Isotope Geochemistry*, Springer, Berlin, Heidelberg, Germany, 173-222, https://doi.org/10.1007/978-3-540-68953-9_6, 2016.
- 560
- Uno, I., Eguchi, K., Yumimoto, K., Takemura, T., Shimizu, A., Uematsu, M., Liu, Z., Wang, Z., Hara, Y., and Sugimoto, N.: Asian dust transported one full circuit around the globe, *Nat. Geosci.*, 2, 557-560, <https://doi.org/10.1038/ngeo583>, 2009.
- Usher, C. R., Michel, A. E., and Grassian, V. H.: Reactions on mineral dust, *Chem. Rev.*, 103, 4883-4940, <https://doi.org/10.1021/cr020657y>, 2003.
- 565
- Wang, X., Hua, T., Zhang, C., Lang, L., and Wang, H.: Aeolian salts in Gobi deserts of the western region of Inner Mongolia: Gone with the dust aerosols, *Atmos. Res.*, 118, 1-9, <https://doi.org/10.1016/j.atmosres.2012.06.003>, 2012.

- Wang, X., Xia, D., Wang, T., Xue, X., and Li, J.: Dust sources in arid and semiarid China and southern Mongolia: Impacts of geomorphological setting and surface materials, *Geomorphol.*, 97, 583-600, <https://doi.org/10.1016/j.geomorph.2007.09.006>, 2008.
- 570 Wang, Y., Yu, W., Pan, Y., and Wu, D.: Acid neutralization of precipitation in Northern China. *Journal of the Air & Waste Management Association*, 62(2), 204-211, <https://doi.org/10.1080/10473289.2011.640761>, 2012.
- Wang, Z., Akimoto, H., and Uno, I.: Neutralization of soil aerosol and its impact on the distribution of acid rain over east Asia: Observations and model results. *Journal of Geophysical Research: Atmospheres*, 107(D19), ACH-6, <https://doi.org/10.1029/2001JD001040>, 2002.
- 575 Wu, F., Cheng, Y., Hu, T., Song, N., Zhang, F., Shi, Z., Hang Ho, S. S., Cao, J., and Zhang, D.: Saltation–sandblasting processes driving enrichment of water-soluble salts in mineral dust, *Environ. Sci. Technol. Lett.*, 9, 921-928, <https://doi.org/10.1021/acs.estlett.2c00652>, 2022.
- Wu, F., Song, N., Hu, T., Ho, S. S. H., Cao, J., and Zhang, D.: Surrogate atmospheric dust particles generated from dune soils in laboratory: Comparison with field measurement, *Particuology*, 72, 29-36, <https://doi.org/10.1016/j.partic.2022.02.007>,
580 2023.
- Wurzler, S., Reisin, T. G., and Levin, Z.: Modification of mineral dust particles by cloud processing and subsequent effects on drop size distributions, *J. Geophys. Res. Atmos.*, 105, 4501-4512, <https://doi.org/10.1029/1999JD900980>, 2000.
- Zhang, D., and Iwasaka, Y.: Size change of Asian dust particles caused by sea salt interaction: Measurements in southwestern Japan, *Geophys. Res. Lett.*, 31, <https://doi.org/10.1029/2004GL020087>, 2004.
- 585 Zhao, Y., Yue, X., Cao, Y., Zhu, J., Tian, C., Zhou, H., Chen, Y., Hu, Y., Fu, W., and Zhao, X.: Multi-model ensemble projection of the global dust cycle by the end of 21st century using the Coupled Model Intercomparison Project version 6 data. *Atmospheric Chemistry and Physics*, 23(13), 7823-7838, <https://doi.org/10.5194/acp-23-7823-2023>, 2023.
- Zhi, M., Wang, G., Xu, L., Li, K., Nie, W., Niu, H., Shao, L., Liu, Z., Yi, Z., Wang, Y., Shi, Z., Ito, A., Zhai, S., and Li, W.: How acid iron dissolution in aged dust particles responds to the buffering capacity of carbonate minerals during Asian
590 Dust Storms, *Environ. Sci. Technol.*, 59, 6167-6178, <https://doi.org/10.1021/acs.est.4c12370>, 2025.
- Zou, X., Li, J., Cheng, H., Wang, J., Zhang, C., Kang, L., Liu, W., and Zhang, F.: Spatial variation of topsoil features in soil wind erosion areas of northern China, *CATENA*, 167, 429-439, <https://doi.org/10.1016/j.catena.2018.05.022>, 2018.